Ab Initio Structures and Stabilities of Doubly Charged Diatomic Metal Helides for the First Row Transition Metals

ARTICLE *in* THE JOURNAL OF PHYSICAL CHEMISTRY A · JULY 2002

Impact Factor: 2.69 · DOI: 10.1021/jp0203503

3 AUTHORS, INCLUDING:

David J D Wilson
La Trobe University
69 PUBLICATIONS **631** CITATIONS

Ab Initio Structures and Stabilities of Doubly Charged Diatomic Metal Helides for the First Row Transition Metals

David J. D. Wilson,[†] Colin J. Marsden,[‡] and Ellak I. von Nagy-Felsobuki*,[†]

Discipline of Chemistry, School of Environmental and Life Sciences, The University of Newcastle, Callaghan, NSW, 2308, Australia and Laboratoire de Physique Quantique, IRSAMC, UMR 5626-CNRS, Université Paul Sabatier, 118, route de Narbonne, F-31062, Toulouse Cedex, France

Received: February 6, 2002; In Final Form: April 19, 2002

The electronic structure and molecular properties of doubly charge transition metal helides, HeX^{2+} (where X = Sc−Cu), have been investigated using the all-electron ROHF−UCCSD(T) method. Basis sets have been developed for the first row transition metals to elucidate trends in bonding, dissociation energies, and vibrational frequencies. The ground state for all the doubly charged helides exhibited a $3d^n$ configuration. In addition, states with configurations that have holes in the metal $3d_\sigma$ orbital exhibited greater binding energies. Relativistic effects have also been investigated using the Cowan-Griffin ansatz. Anharmonic vibrational frequencies have been determined variationally.

I. Introduction

The unique chemistry of helium has been largely unraveled due to theoretical studies.[1−10] Frenking, Koch and co-workers[3−6] have extensively detailed the electronic structure of singly and doubly charged helide ions, containing first and second row elements. These workers have employed a donor−acceptor model in order to elucidate the binding nature of these helide ions.[3−6] It was found that the singly charged species in the ground state were van der Waals complexes, stabilized by charge-induced interactions. In the case of the respective excited states, the covalent character of the bond became more significant. For the doubly charged species, the bonding in the ground state was determined to be covalent. Frenking, Koch, and co-workers[3−6] found that the strength of the He-X bond was primarily determined by the electronic structure rather than by the charge or electronegativity of the helium binding partner. Radom, Wong, and co-workers[9,10] have also examined many similar species employing a qualitative MO approach. To rationalize the nature of the helium binding trends, they have focused on the respective occupations of the bonding, antibonding, and nonbonding MOs. They showed that highly charged carbon and silicon helides exhibited surprising stability.[9−10]

Over the last two decades, there has been considerable experimental[11−16] and theoretical[1−2,16−22] interest in transition metal (TM) ion rare-gas (RG) chemistry. In a comprehensive review, Harrison[23] has highlighted the difficulties and necessary requirements of theoretically investigating transition metal diatomics. Bauschlicher and co-workers[2,17−21] have theoretically examined the binding of helium to singly charged first row TM cations. It would be anticipated that the RG-TM^+ binding energy would be largely determined by charge-induced dipole interactions. However, these workers found that electrostatic reasoning alone was insufficient to explain helium binding.[16]

There have been few experimental investigations of transition metal helides. Bowers and co-workers[11,12] have employed an electronic state chromatographic technique in order to determine accurate binding energies for a variety of RG-TM^+ systems (where the TM = Cr^+, Co^+, and Ni^+). Müller, Tsong, and co-workers[13−15] using field-ion-microscopy have reported the existence of RG-TM molecular ions, such as HeM^{2+} (where *M* = V, Fe, Ta, Mo, Rh, Pt, Ir, etc.), HeM^{3+} (where *M* = V, Ta, W, Re, Ir, etc.), He_2Pt^{2+}, He_2W^{3+}, He_3W^{3+}, and He_4W^{3+}. The latter technique uncovered the existence of highly charged species.

As an extension of our continuing investigation of the structure and stabilities of helide ions,[7,8] we wish to report on the ab initio investigation of doubly charged diatomic TM helides. Thus far, there have been no thorough and systematic investigations of these doubly charged species in the literature. To date, the only theoretical investigation is a CASSCF study of He−Ti^{2+} by Hotokka and co-workers.[1] In the present study, we shall elucidate bonding and binding trends of these transition metal helides (including some spectroscopic properties). With the development of new experimental techniques,[11−15] it is hoped that the results reported here will encourage further experimental and theoretical investigation of these novel species.

II. Computational Procedure

Within the GAUSSIAN 98 suite of programs,[24] the unrestricted Hartree−Fock (UHF) and coupled cluster single and double excitation with perturbative triples (CCSD(T)) methods were utilized for the calculation of atomic polarizability, excited-state transition energies, ionization energies, and molecular structures. Unrestricted (UCCSD(T)) and restricted (RCCSD(T)) methods were employed for open and closed shell systems, respectively. Within MOLPRO,[27] the restricted open-shell HF (ROHF), restricted Kohn−Sham (RKS) B3LYP, the unrestricted CCSD(T) method based on an ROHF reference wave function (U_RCCSD(T))[25,26] and the internally contracted multireference configuration interaction (ICMRCI) were employed. The appropriateness of employing single reference methods was

* To whom all correspondence should be addressed: E-mail: ellak@newcastle.edu.au Phone: +61 2 4921 5482. Fax: +61 2 4921 6923.
† Discipline of Chemistry, School of Environmental and Life Sciences, The University of Newcastle.
‡ Laboratoire de Physique Quantique, IRSAMC, UMR 5626-CNRS, Université Paul Sabatier.

10.1021/jp0203503 CCC: $22.00
Published on Web 07/24/2002

investigated via the T_1 diagnostic of Lee and co-workers.[28] All electrons were included in all the correlation calculations.

To reduce basis set superposition errors (BSSE) and provide accurate atomic polarizabilities α, (i.e., two necessary properties for accurately describing weakly bound systems) large primitive basis sets are required.

For helium, the aug-cc-pVQZ set of Woon and Dunning[29] was employed, with the most diffuse *s*, *p*, *d* functions and all the *f* functions removed and replaced with even-tempered *s*,*p*,*d* functions to produce a basis set contraction of [6*s*5*p*3*d*]. At the CCSD(T) level of theory (Gaussian 98), the atomic polarizability, ionization energy (IE) and $^1S \leftarrow {}^3S$ electronic transition of helium have been determined to be 1.385 au, 24.55 and 19.79 eV in excellent agreement with the experimental values of 1.384 au,[30] 24.59 eV,[31] and 19.82 eV,[32] respectively. In comparison, employing the aug-cc-pVQZ basis at the same level of theory yields the atomic polarizability, IE and $^1S \leftarrow {}^3S$ electronic transition energy of helium to be 1.384 au, 24.57 and 19.86 eV, respectively. U_RCCSD(T) results for the ionization and $^1S \leftarrow {}^3S$ transition energy replicated the Gaussian 98 results. Hence, the constructed basis set is an adequate substitute for the more CPU-expensive aug-cc-pVQZ set.

For the first row transition-metals, Wachters+f [8*s*, 6*p*, 4*d*, 1*f*] basis set[33,34] was used. This set was modified and extended, with Wachters *d* functions replaced with the 6*d* primitive set (contracted to 3*d* with a 4/1/1 contraction) of Rappe and co-workers[35] because Hay[36] has shown that the Wachters+f basis set poorly describes molecular systems. Langhoff and Bauschlicher[37] have indicated that a flexible *d* contraction would be more significant than diffuse *f* functions to enable accurate recovery of the correlation energy. However, these workers have also recommended the inclusion of both tight and diffuse *f* functions to accurately describe bonding. Subsequently, the *p*-space and *d*-space were both expanded by the addition of two diffuse functions, added in an even-tempered manner with a ratio of 2.5 from the most diffuse *p* and *d* function, respectively. The most diffuse *f* function was uncontracted and a single *g* function added with a ratio of 1.2 to the largest *f* exponent as suggested by Almlof and Taylor.[38] The final contracted basis set has the form, [8*s*, 7*p*, 5*d*, 2*f*, 1*g*]. Such a contraction is expected to approach the basis set limit. Moreover, we expect these basis sets to be approximately equal in quality for all the transition metals investigated, therefore giving credence to computed trends. Only the pure spherical components of the basis functions were included in all calculations. These basis sets are available upon request from the authors.

Equilibrium geometries, harmonic frequencies, and dissociation energies were determined at the ROHF, RKS−B3LYP, and U_RCCSD(T) level of theory, employing the direct module of MOLPRO.[39] For all geometry optimizations, stationary points on the potential surface were characterized by calculating the harmonic frequencies. This was achieved by a quadratic fit to points about the potential minimum. BSSE effects were examined using the counterpoise method.[40]

Potential energy curves were constructed for the low-lying states of the first row $HeTM^{2+}$ species at the U_RCCSD(T) level of theory. The solution algorithm has been detailed elsewhere.[41] Typically, 20−30 discrete points on the energy hypersurface were fitted using a Simons-Parr-Finlan power series function. The potential function was embedded into a one-dimensional vibrational Hamiltonian, which was solved variationally. The finite-element-method was employed using a 16-point Gauss-Legendre quadrature scheme. All potential integrals were evaluated using the Harris, Engerholm and Gwinn scheme.[41]

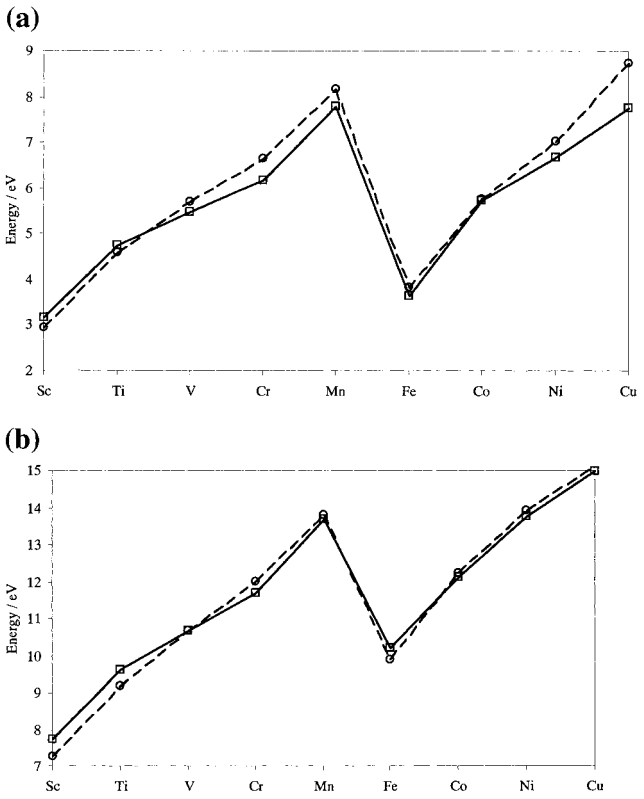

Figure 1. Atomic transition energies for first row transition metal dipositive ions. (a) $3d^n - 3d^{n-1}4s$ transitions and (b) $3d^n - 3d^{n-1}4p$ transitions. Experimental[32] (square markers) and U_RCCSD(T) results (circle markers).

Convergence criteria were employed for the variational solution of the anharmonic vibrational states to ensure decay of the wave function in the classically forbidden region and convergence of the low-lying vibrational states.

Relativistic effects were investigated within the Cowan−Griffin scheme.[42] Martin[43] has shown that the first-order perturbational Cowan−Griffin relativistic operator provides a "good" approximation to the full Dirac-HF operator for many-atom systems. (For a more complete treatment of relativistic effects, spin−orbit coupling effects would also need to be taken into account). Identical discrete points (see above) on the potential energy hypersurface were calculated using this relativistic scheme.[42] Analytical potential functions were constructed using Simons−Parr−Finlan power series functions, with anharmonic vibration energy levels determined variationally using the same solution algorithm as outlined above for the nonrelativistic calculations.

III. Results and Discussion

A necessary requirement of the theoretical models employed is the agreement between experimental and calculated values of the atomic transition energies for low-lying $3d^n4s^m4p^l$ states of TM^{2+} ions. In contrast to the neutral and singly charged TM atoms (where the $3d^{n-2}4s^2$ and $3d^{n-1}4s$ configurations are the most significant) it would be expected that the $3d^{n-1}4s$ and $3d^n$ configurations dominate the wave function for the doubly charged species (with a ground-state configuration of $3d^n$ for all first row TM^{2+}). Moreover, $3d^{n-1}4p$ configurations are expected to be of greater significance than $3d^{n-2}4s^2$ configurations for recovering correlation energy.

Experimental energies for $3d^n \leftarrow 3d^{n-1}4s$ and $3d^n \leftarrow 3d^{n-1}4p$ transitions are presented in Figure 1. The $3d^n \leftarrow 3d^{n-1}4s$

TABLE 1: Experimental and ROHF, RKS−B3LYP and U_RCCSD(T) Calculated $3d^n \leftarrow 3d^{n-1}4s$ and $3d^n \leftarrow 3d^{n-1}4p$ Atomic Transition Energies (eV) for First Row Transition Metal Dications[a]

species	transition	ROHF	B3LYP	CCSD(T)	expt[b]
		$3d^n \leftarrow 3d^{n-1}4s$			
Sc^{2+}	$^2D - {}^2S$	3.28	3.88	2.96	3.17
Ti^{2+}	$^3F - {}^3D$	4.65	5.17	4.60	4.74
V^{2+}	$^4F - {}^4F$	5.65	5.91	5.71	5.49
Cr^{2+}	$^5D - {}^5F$	6.59	6.75	6.65	6.19
Mn^{2+}	$^6S - {}^6D$	8.19	7.97	8.18	7.79
Fe^{2+}	$^5D - {}^7S$	2.82	4.76	3.84	3.65
Co^{2+}	$^4F - {}^6D$	4.55	6.29	5.77	5.73
Ni^{2+}	$^3F - {}^5F$	5.81	7.13	7.04	6.69
Cu^{2+}	$^2D - {}^4F$	7.51	8.63	8.75	7.75
	MAD (eV)	*0.48*	*0.59*	*0.33*	
	MRD (eV)	*-0.24*	*0.59*	*0.26*	
		$3d^n \leftarrow 3d^{n-1}4p$			
Sc^{2+}	$^2D - {}^2P^0$	7.47	7.97	7.28	7.73
Ti^{2+}	$^3F - {}^3F^0$	9.04	9.51	9.18	9.64
V^{2+}	$^4F - {}^4G^0$	10.48	10.67	10.67	10.68
Cr^{2+}	$^5D - {}^5G^0$	11.87	12.02	12.03	11.71
Mn^{2+}	$^6S - {}^6F^0$	13.45	13.47	13.82	13.72
Fe^{2+}	$^5D - {}^7P^0$	8.72	10.70	9.90	10.22
Co^{2+}	$^4F - {}^6D^0$	10.90	12.70	12.24	12.12
Ni^{2+}	$^3F - {}^5F^0$	12.61	13.99	13.96	13.79
Cu^{2+}	$^2D - {}^4D^0$	13.77	14.95	15.14	15.00
	MAD (eV)	*0.71*	*0.25*	*0.28*	
	MRD (eV)	*−0.70*	*0.15*	*−0.04*	
		including all results			
	MAD (eV)	*0.61*	*0.42*	*0.28*	
	MRD (eV)	*−0.47*	*0.37*	*0.11*	

[a] Errors are given as mean absolute deviation (MAD) and mean relative deviation (MRD). See main text for computational details. [b] Moore (ref 32).

transition energies (Figure 1a) can be understood in terms of two competing effects. First, there is an increased stabilization of the 3*d* orbital relative to the 4*s* orbital from Sc to Cu due to an increase in nuclear charge. Second, the preference for high-spin *d* shells is observed as a consequence of the large gain in the exchange energy due to an increasing number of compact *d* orbitals as one goes from Sc−Cu. For Sc−Mn, both these effects differentially stabilize the $3d^n$ configuration, ensuring a monotonic increase in the $3d^n \leftarrow 3d^{n-1}4s$ transition energy. For Fe^{2+}, the $3d^5 4s$ configuration is stabilized in comparison with the $3d^6$ configuration due to the loss of exchange energy that is obtained by coupling the sixth 3*d* electron into the high-spin $3d^5$ configuration. However, this loss is not sufficient to overcome the differential gain that is obtained from occupying the stable 3*d* orbital. Hence, the $3d^6$ configuration remains lower in energy although there is a reduction in the $3d^6 \leftarrow 3d^5 4s$ transition energy. For Co−Cu, a steady increase in the transition energy is again observed, due to the increased stabilization of the 3*d* orbital relative to the 4*s* orbital. Similarly, this analysis is consistent with the trends observed for $3d^n \leftarrow 3d^{n-1}4p$ transitions.

As a test of the suitability of single reference methods, all-electron ROHF, RKS−B3LYP and U_RCCSD(T) methods have been employed to calculate these electronic transitions (and compared to the *j*-averaged experimental data from Moore[32]). The calculated transition energies, mean absolute deviations (MAD) and mean relative deviations (MRD) from the experimental data are presented in Table 1. The U_RCCSD(T) results are further compared to experimental data in Figure 1 for the $3d^n \leftarrow 3d^{n-1}4s$ and $3d^n \leftarrow 3d^{n-1}4p$ transitions. The RKS−B3LYP method is seen to consistently overestimate the transition energy, as evidenced by the agreement between MAD and MRD. The U_RCCSD(T) method duly reproduces experimental values, with a coincidental cancellation of errors responsible for a near-zero MRD for $3d^n \leftarrow 3d^{n-1}4p$ transitions. It is interesting to note that the RKS−B3LYP results are comparable to the U_RCCSD(T) results for the $3d^{n-1}4p$ configurations, but that the RKS−B3LYP MAD is nearly double that of the U_R-CCSD(T) method for the $3d^{n-1}4s$ configurations. Thus, the accuracy and stability of the U_RCCSD(T) method is more than satisfactory (i.e., the order of the states is correct and the computed separations between the states are in good agreement with experimental data).

Bauschlicher and Langhoff[21] have noted that the error in a calculation is usually increased when relativistic effects are included due to the bias in the computational method being exaggerated by the corrections. Due to the 4*s* orbital being smaller in radial extent than the 3*d* orbitals, relativistic effects will preferentially stabilize the 4*s* orbital, possibly to the extent of rearranging electronic states. For all first row atomic TM^{2+} ions, the ground state $3d^n$ configuration is significantly lower in energy than states arising from $3d^{n-1}4s$, $3d^{n-2}4s^2$, and $3d^{n-1}4p$ configurations. Hence, this preferential stabilization is not expected to be sufficient to rearrange electronic states and thus relativistic effects can reasonably be estimated in a perturbative manner from the reference ROHF wave function.[42,43] The addition of relativistic corrections to the U_RCCSD(T) energies alters the MAD (MRD) for the TM^{2+} $3d^n \leftarrow 3d^{n-1}4s$ and $3d^n \leftarrow 3d^{n-1}4p$ transitions to 0.30 (0.18) and 0.31 (0.31) eV, respectively. There appears a significant increase in the MRD of the $3d^n \leftarrow 3d^{n-1}4p$ transitions (with little difference in the MAD), indicating that fortuitous cancellation of errors has occurred for the nonrelativistic results. Incorporating all calculated transitions, the MAD (MRD) becomes 0.32 (0.25) eV. These results support the notion that the inclusion of relativistic effects increases errors. However, for these systems the increase is marginal for the states investigated.

Examination of the T_1 diagnostic[28] for each TM^{2+} ion configuration suggests that single reference methods are suitable for all the ground-state ions (with typical T_1 values of the order of 0.005 and with the largest value of 0.0087 for the ^4F ($3d^7$) state of Co^{2+}). Similar results were obtained for $3d^{n-1}4p$ and $3d^{n-1}4s$ configurations. However, it should be noted that multireference methods would be required to accurately describe excited states, where significant mixing of $3d^n$ orientations, along with $3d^{n-1}4s$, $3d^{n-1}4p$ and $3d^{n-2}4s^2$ configurations could be expected to occur.

The bonding in RG-TM ion systems is primarily expected to be electrostatic, with the most important term being the charge-induced-dipole $[q^2\alpha/(2r^4)]$. Here, q is the TM ion charge, α is the RG polarizability, and r is the internuclear separation between the TM ion and the RG atom. Thus, the binding energy is a function of both the RG polarizability and the interatomic distance. However, as described by Partridge, Langhoff, and Bauschlicher,[17] there are several metal-centered effects that can enhance bonding via a reduction in metal−ligand repulsion. Predominantly, mechanisms that minimize occupation of the antibonding 4*s* and $3d_\sigma$ metal orbitals, reduces metal ion-ligand repulsion. For systems whereby the metal 4*s* orbital is occupied, *sp* and/or sd_σ hybridization and *s* to *d* promotion can reduce repulsion. For $3d^n$ occupied metal ions, both orientation of the 3*d* open-shell orbital and sd_σ hybridization affect metal−ligand repulsion. The high IE of the TM^{2+} ions may also lead to significant He to TM ion charge donation. For first row TM atoms Sc−Cu, the second IE (IE_2) is smaller than the first IE (IE_1) of He. Hence, all $HeTM^{2+}$ would be expected to dissociate

TABLE 2: All-electron ROHF, RKS−B3LYP, and U_RCCSD(T) Optimized Structures and All-electron U_RCCSD(T) Calculated Transition Energies, Metal Charges, Dissociation Energies, Harmonic Vibrational Frequencies, and Zero Point Energies of the Low-Lying States of HeX^{2+} (X = Sc−Cu)

species	state	configuration		R_e(Å) ROHF	R_e(Å) B3LYP	R_e(Å) CCSD(T)	T_e kJ mol^{-1}	metal charge/e	D_e[a] kJ mol^{-1}	ω_e cm^{-1}	ZPE kJ mol^{-1}
$HeSc^{2+}$	$^2\Delta$	$3d^1$	$3d_\delta^1$	2.272	2.197	2.189	0.00[b]	1.91	20.4	372	2.2
	$^2\Pi$	$3d^1$	$3d_\pi^1$	2.259	2.160	2.149	-0.69	1.91	18.7	365	2.1
	$^2\Sigma^+$	$3d^1$	$3d_\sigma^1$	2.671	2.503	2.465	11.59	1.95	5.4	239	1.4
$HeTi^{2+}$[c]	$^3\Phi$	$3d^2$	$3d_\pi^1 d_\delta^1$	2.149	2.072	2.065	0.00	1.90	25.5	412	2.4
	$^3\Delta$	$3d^2$	$3d_\sigma^1 3d_\delta^1$	2.457	2.337	2.315	19.20	1.94	14.2	300	1.8
	$^3\Pi$	$3d^2$	$3d_\sigma^1 3d_\pi^1$	2.390	2.248	2.219	73.15	1.93	21.4	326	2.1
HeV^{2+}	$^4\Delta$	$3d^3$	$3d_\pi^2 3d_\delta^1$	2.053	1.956	1.965	0.00	1.91	30.5	457	2.7
	$^4\Pi$	$3d^3$	$3d_\pi^1 3d_\delta^2$	2.248	2.130	2.067	11.55	1.93	17.0	364	2.2
	$^4\Phi$	$3d^3$	$3d_\sigma^1 3d_\pi^1 3d_\delta^1$	2.325	2.197	2.197	31.53	1.95	11.0	341	2.5
$HeCr^{2+}$	$^5\Sigma^+$	$3d^4$	$3d_\pi^2 3d_\delta^2$	1.977	1.877	1.881	0.00	1.87	36.5	526	3.2
	$^5\Pi$	$3d^4$	$3d_\sigma^1 3d_\pi^1 3d_\delta^2$	2.200	2.097	2.086	16.68	1.93	21.8	387	2.3
	$^5\Delta$	$3d^4$	$3d_\sigma^1 3d_\pi^2 3d_\delta^1$	2.215	2.086	2.076	17.93	1.93	20.5	374	2.2
$HeMn^{2+}$	$^6\Sigma^+$	$3d^5$	$3d_\sigma^1 3d_\pi^2 3d_\delta^2$	2.116	2.007	2.004	0.00	1.93	25.8	414	2.5
	$^4\Pi$	$3d^5$	$3d_\pi^3 3d_\delta^2$	1.929	1.830	1.817	347.29	1.88	39.9[d]	546	3.3
	$^4\Gamma$	$3d^5$	$3d_\sigma^1 3d_\pi^2 3d_\delta^2$	2.107	1.995	1.991	362.17	1.93	26.8[d]	422	2.5
	$^4\Phi$	$3d^5$	$3d_\sigma^1 3d_\pi^3 3d_\delta^1$	2.052	1.935	2.002	405.99	1.93	18.3[d]	362	2.3
	$^4\Delta$	$3d^5$	$3d_\sigma^1 3d_\pi^2 3d_\delta^2$	2.093	1.983	1.983	406.40	1.92	26.7[d]	428	2.5
$HeFe^{2+}$	$^5\Delta$	$3d^6$	$3d_\sigma^1 3d_\pi^2 3d_\delta^3$	2.022	1.931	1.923	0.00	1.93	32.8	473	2.8
	$^5\Pi$	$3d^6$	$3d_\sigma^1 3d_\pi^3 3d_\delta^2$	2.020	1.908	1.904	0.83	1.92	32.0	466	2.8
	$^5\Sigma^+$	$3d^6$	$3d_\sigma^2 3d_\pi^2 3d_\delta^2$	2.229	2.096	2.103	14.45	1.97	19.7	345	2.1
	$^3\Phi$	$3d^6$	$3d_\pi^3 3d_\delta^3$	1.880	1.782	1.840	265.90	1.91	57.1	515	2.4
$HeCo^{2+}$	$^4\Phi$	$3d^7$	$3d_\sigma^1 3d_\pi^3 3d_\delta^3$	1.940	1.845	1.842	0.00	1.93	38.4(789)[e]	523	3.1
	$^4\Pi$	$3d^7$	$3d_\sigma^2 3d_\pi^3 3d_\delta^2$	2.080	1.972	1.949	2.94	1.97	36.2(692)	352	2.2
	$^4\Delta$	$3d^7$	$3d_\sigma^2 3d_\pi^2 3d_\delta^3$	2.118	[f]	2.008	7.02	1.96	31.2(806)	400	2.4
$HeNi^{2+}$	$^3\Delta$	$3d^8$	$3d_\sigma^1 3d_\pi^4 3d_\delta^3$	1.877	1.772	1.775	0.00	1.94	42.8(703)	550	3.3
	$^3\Phi$	$3d^8$	$3d_\sigma^2 3d_\pi^3 3d_\delta^3$	2.038	1.900	1.940	39.33	1.97	28.8(662)	435	2.6
$HeCu^{2+}$	$^2\Sigma^+$	$3d^9$	$3d_\sigma^1 3d_\pi^4 3d_\delta^4$	1.816	1.717	1.722	0.00	1.87	51.2(493)	604	3.6
	$^2\Pi$	$3d^9$	$3d_\sigma^2 3d_\pi^3 3d_\delta^4$	1.962	1.869	1.880	18.18	1.93	34.3(475)	481	2.6
	$^2\Delta$	$3d^9$	$3d_\sigma^2 3d_\pi^4 3d_\delta^3$	1.969	1.859	1.877	20.17	1.92	32.3(473)	463	2.8

[a] Calculated as $HeTM^{2+} \rightarrow He + TM^{2+}$. [b] (IC)MRCI results indicate that the $^2\Delta$ state is lower than the $^2\Pi$ state by 0.77 kJ mol^{-1}. [c] Hotokka et al.[1] employing CASSCF methods determined R_e to be 2.052 Å, with a Mulliken He population of 1.94 e, D_e of 16.1 kJ mol^{-1}, ω_e of 489 cm^{-1}, and ZPE of 2.4 kJ mol^{-1}. [d] Quartet state dissociation energies calculated with respect to the atomic ^{4}G ($3d_\sigma^1 3d_\pi^2 3d_\delta^2$) Mn^{2+} state. [e] Bracketed values refer to the negative of energy of dissociation into the charge separated products $HeTM^{2+} \rightarrow He^+ + TM^+$. [f] Unbound.

to $He + TM^{2+}$. Dissociation into the charge separated products $He^+ + TM^+$ was considered for the later members of the Sc−Cu series with IE_2 approaching the IE_1 of He.

The equilibrium geometries for selected low-lying states of the $HeTM^{2+}$ ions determined at the ROHF, RKS−B3LYP, and U_RCCSD(T) level of theory are summarized in Table 2 and illustrated in Figure 2. It is of interest to note that for equilibrium geometries, the RKS−B3LYP results exactly mirror the U_R-CCSD(T) equilibrium geometries, whereas the ROHF method consistently overestimates the bond length. Electronic transition energies, metal charge, dissociation energies, harmonic vibrational frequencies and zero-point-energies (ZPE) for low-lying states of $HeTM^{2+}$ are also presented in Table 2 at the U_RCCSD-(T) level of theory. The metal charge is determined from a Mulliken population analysis and is equivalent to the helium electron population. These values provide a useful qualitative description of the strength of the helium bond.

The ground state for all the doubly charged helides exhibit a $3d^n$ configuration at the ROHF, RKS−B3LYP, and U_RCCSD-(T) levels of theory. The electronic state-determining factor is found to be the orientation of the occupied 3*d* orbitals, with states described by electronic configurations exhibiting holes in the $3d_\sigma$ orbital favored. The $3d_\sigma$ orbital is antibonding between He and TM^{2+}, even though the contribution of helium is small.

For $HeSc^{2+}$, the ground state arises from a singly occupied Sc 3*d* orbital. However, while states arising from the $3d_\sigma^1$ configuration are higher in energy, the $3d_\pi^1$ and $3d_\delta^1$ configurations are nearly degenerate due to the lack of occupied *p* orbitals in the He atom. At the ROHF level, the $^2\Delta$ state is lower by only 94.2 cm^{-1}, whereas the RKS−B3LYP and U_RCCSD(T) levels reverse the order of states with the $^2\Pi$ state ($3d_\pi^1$) lower in energy than the $^2\Delta$ state ($3d_\delta^1$) by 4.7 and 57.7 cm^{-1}, respectively. This is supported by ICMRCI results. On the basis of a state-averaged MCSCF reference wave function (which includes the 4*s* and 3*d* orbitals in the valence space and the Davidson correction to the energy) the $^2\Pi$ state is determined to be lower in energy by 16.8 cm^{-1}. As an upper bound, it is expected that these states differ in energy by only 1 kJ mol^{-1} (ca. 84 cm^{-1}). Hence, these two states are too close to degeneracy to unambiguously assign ground-state symmetry.

To examine the effect of correlating all electrons, frozen-core calculations were carried out for electronic states of $HeSc^{2+}$ arising from a $3d^1$ configuration. The equilibrium bond lengths for the $^2\Delta$, $^2\Pi$, and $^2\Sigma^+$ states were determined to be 2.266, 2.235 and 2.619 Å with a 1*s*2*s*2*p*3*s*3*p* frozen core, and 2.192, 2.151, and 2.482 with a 1*s*2*s*2*p* frozen core, respectively. This compares to the all-electron bond lengths of 2.189, 2.149, and 2.465 Å, respectively. The 1*s*2*s*2*p*3*s*3*p* (and 1*s*2*s*2*p*) frozen-core results are longer than the all-electron results (presented in Table 2) by 0.077 (0.043), 0.086 (0.002), and 0.154 (0.017) Å. Charge donation further reflects this result. The respective 1*s*2*s*2*p*3*s*3*p* and 1*s*2*s*2*p* frozen-core, and all-electron helium charge donation was determined to be 0.074, 0.087, and 0.087 for the $^2\Delta$ state, 0.076, 0.088, and 0.088 for the $^2\Pi$ state and 0.037, 0.048, and 0.050 for the $^2\Sigma^+$ states. Hence, the inclusion of all electrons in the correlation calculation reduces the bond length of $HeSc^{2+}$ by ca. 0.008 Å and increases He charge donation by ca. 0.01 electrons, compared to the 1*s*2*s*2*p*3*s*3*p* frozen-core results. The increase in bond length is particularly evident for states with an occupied $3d_\sigma$ orbital, where it is clear

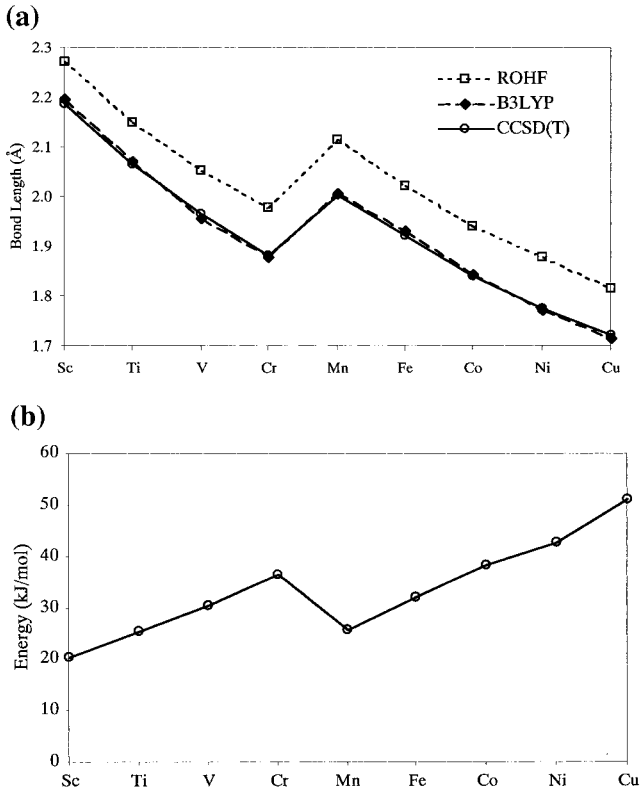

Figure 2. (a) Optimized bond distances (Angstroms) and (b) dissociation energies (kJ mol^{-1}) for the electronic ground states of HeX^{2+} (X = Sc−Cu). See Table 2 for description of states.

that the inclusion of at least the 3*s* and 3*p* orbitals in the valence space is needed to cater for the mechanisms that minimize occupation of the 4*s* and $3d_\sigma$ metal orbitals such as sd_σ hybridization. Significantly, the ordering of states is the same for the frozen-core and all-electron results for $HeSc^{2+}$. This is also mirrored for the other $HeTM^{2+}$ species, although the bond length contraction is found to generally diminish from Sc to Cu as the number of 3*d* occupied orbitals increases.

The ground state of $HeTi^{2+}$ is the $^3\Phi$ state, described by the $3d_\pi^1 3d_\delta^1$ configuration. States arising from configurations, with an occupied $3d_\sigma$ orbital, are significantly higher in energy. An increase in binding energy from Sc to Ti is observed, corresponding to a smaller internuclear distance for $HeTi^{2+}$. In the only other reported study of $HeTi^{2+}$, Hotokka and co-workers,[1] employing CASSCF methods have optimized the $^3\Phi$ ground-state geometry of $HeTi^{2+}$. In a test of the accuracy of their methodology, they determined the IE_1 of He to be 24.00 eV compared to the experimental value of 24.59 eV. They also determined the first and second IEs of Ti to be 6.46 and 12.93 eV[1] compared to the experimental values of 6.83 and 13.63 eV,[31] respectively. The CCSD(T) calculated results are 6.73 and 13.45 eV, respectively. Hotokka and co-workers[1] have determined the $HeTi^{2+}$ equilibrium bond length to be 2.052 Å, with a Mulliken He population of 1.94 e, D_e of 16.05 kJ mol^{-1}, harmonic vibrational frequency of 489 cm^{-1} and ZPE of 2.42 kJ mol^{-1}. This is in good agreement with the results presented that are expected to have a higher level of accuracy.

For HeV^{2+}, the ground state is determined to be the $^4\Delta$ state described by the $3d_\pi^2 3d_\delta^1$ configuration. The minimization of the TM-ligand repulsion (i.e., TM-ligand stabilization) gained from an empty $3d_\sigma$ orbital is sufficient to change the TM^{2+} 3*d* orientation from the ground-state atomic ion $3d_\sigma^1 3d_\pi^1 3d_\delta^1$ configuration. The $^4\Pi$ state is not adequately treated with an SCF wave function, being a mix of the $3d_\pi^1 3d_\delta^2$ and $3d_\sigma^1 3d_\pi^1 3d_\delta^1$ configurations. From TM-ligand stabilization arguments, it would be expected to lie lower than the $^4\Phi$ state ($3d_\sigma^1 3d_\pi^1 3d_\delta^1$). The shorter bond length determined for the $^4\Pi$ state (being closer to the $^4\Delta$ state bond length) supports the expected order of states. However, the $^4\Pi$ state is determined to be significantly higher in energy as a result of the inadequacy of single reference methods for this state (which is generally poor for other than the ground electronic states).

The lowest lying electronic states of $HeCr^{2+}$ derive from a $3d^4$ occupation, with $3d^3 4s$ occupied states significantly higher in energy. The $^5\Sigma^+$ ground state of $HeCr^{2+}$ arises from a $3d_\pi^2 3d_\delta^2$ configuration, in contrast to atomic Cr^{2+}, which possesses a ^{5}D ($3d_\sigma^1 3d_\pi^2 3d_\delta^1$) ground state. The $^5\Sigma^+$ molecular state is stabilized due to the empty $3d_\sigma$ orbital, reducing TM-ligand repulsion. Low-lying $^5\Delta$ ($3d_\sigma^1 3d_\pi^2 3d_\delta^1$) and $^5\Pi$ ($3d_\sigma^1 3d_\pi^1 3d_\delta^2$) states are higher in energy and quasi-degenerate due to the same $3d_\sigma$ shell occupation.

For $HeMn^{2+}$, the ground state is determined to be the $^6\Sigma^+$ state described by the $3d_\sigma^1 d_\pi^2 3d_\delta^2$ configuration. Excited states that derive from configurations with an empty $3d_\sigma$ orbital, such as $^4\Pi$ ($3d_\pi^3 3d_\delta^2$) and $^4\Delta$ ($3d_\pi^2 3d_\delta^3$) exhibit significantly shorter bond lengths. However, the TM-ligand stabilization energy gained from an empty $3d_\sigma$ orbital is insufficient to overcome the preference for high-spin $3d^n$ configurations. It would be expected that the low spin $^4\Delta$ and $^4\Pi$ states should be close in energy. However, this is not observed. The $^4\Pi$ state configuration is more adequately represented by an SCF reference wave function than the $^4\Delta$ state, which is a mix of $3d_\sigma^1 3d_\pi^2 3d_\delta^2$ and $3d_\pi^2 3d_\delta^3$ configurations. The lowest quartet state of atomic Mn^{2+} is ^{4}G ($3d_\sigma^1 3d_\pi^2 3d_\delta^2$), with the analogous molecular $^4\Gamma$ state found to be slightly higher in energy than the $^4\Pi$ state but lower than any other quartet state with an occupied $3d_\sigma$ orbital.

The ground state of $HeFe^{2+}$ is the $^5\Delta$ ($3d_\sigma^1 3d_\pi^2 3d_\delta^3$) state, analogous to the ground ^{5}D state of the Fe^{2+} ion. High spin $3d^6$ states $^5\Pi$ ($3d_\sigma^1 3d_\pi^2 3d_\delta^2$) and $^5\Sigma^+$ ($3d_\sigma^2 3d_\pi^2 3d_\delta^2$) are higher in energy with longer bond lengths. The low-spin $^3\Phi$ state is poorly described at the SCF level because this state is a mix of $3d_\pi^3 3d_\delta^3$ and $3d_\sigma^2 3d_\pi^3 3d_\delta^1$ configurations. At the CCSD(T) level of theory, the $^3\Phi$ state exhibits a much shorter bond length than the $^5\Delta$, $^5\Sigma^+$ or $^5\Pi$ states but the gain in TM-ligand binding energy is insufficient to overcome the loss of exchange energy with a low-spin configuration. Hence, the $^3\Phi$ state is found to lie 265.9 kJ mol^{-1} above the $^5\Delta$ ground state.

The ground state of $HeCo^{2+}$ is determined to be $^4\Phi$ arising from a $3d_\sigma^1 3d_\pi^3 3d_\delta^3$ configuration. The $^4\Delta$ ($3d_\sigma^2 3d_\pi^2 3d_\delta^3$) and $^4\Pi$ ($3d_\sigma^2 3d_\pi^3 3d_\delta^2$) states are higher in energy and moreover exhibit longer bond lengths and decreased charge donation to the metal, due to the doubly occupied $3d_\sigma$ orbital.

The $HeNi^{2+}$ ground state is determined to be $^3\Delta$ ($3d_\sigma^1 3d_\pi^4 3d_\delta^3$) favored due to the $3d_\sigma$ hole. This is in contrast to atomic Ni^{2+}, which is found to have a ^{3}F ground state described by the symmetric $3d_\sigma^2 3d_\pi^3 3d_\delta^3$ configuration.[32] The analogous $^3\Phi$ molecular state is found to be higher in energy. The $^3\Pi$ state is poorly described at the HF level of theory, being a mix of the $3d_\sigma^2 3d_\pi^3 3d_\delta^3$ and $3d_\sigma^1 3d_\pi^3 3d_\delta^4$ configurations. This state would be expected to exhibit a shorter bond length than the $^3\Phi$ state, but longer than the ground $^3\Delta$ state.

This same effect is observed for $HeCu^{2+}$, which has been determined to have a ground state of $^2\Sigma^+$ described by $3d_\sigma^1 3d_\pi^4 3d_\delta^4$ in contrast to the ground state ^{2}D of atomic Cu^{2+} described by $3d_\sigma^2 3d_\pi^4 3d_\delta^3$. The $HeCu^{2+}$ $^2\Delta$ ($3d_\sigma^2 3d_\pi^4 3d_\delta^3$) and $^2\Pi$ ($3d_\sigma^2 3d_\pi^3 3d_\delta^4$) states are found to be 0.21 and 0.19 eV above the $^2\Sigma^+$ ground state at the U_RCCSD(T) level of theory, respectively. For He with no occupied *p* orbitals, the different

TABLE 3: Variational Anharmonic Spectroscopic Properties (determined from fits to the potential curves) of Ground States and Selected Low-lying Excited States of HeX^{2+} (X=Sc−Cu)

		relativistic				non relativistic						
species		R_e (Å)	$\nu_{1\rightarrow0}$ (cm^{-1})	ZPE (kJ/mol)	ratio[a]	R_e (Å)	$\nu_{1\rightarrow0}$ (cm^{-1})	ZPE (kJ/mol)	ratio[a]	ω_e (cm^{-1})	$\omega_e\chi_e$ (cm^{-1})	bound states[b]
$HeSc^{2+}$	$^2\Delta$	2.189	332	2.14	0.90	2.193	330	2.13	0.90	365.3	16.8	4
$HeTi^{2+}$	$^3\Phi$	2.061	381	2.43	0.92	2.067	378	2.42	0.92	411.3	15.6	8
HeV^{2+}	$^4\Delta$	1.958	425	2.71	0.93	1.965	421	2.69	0.92	457.5	18.2	7
$HeCr^{2+}$	$^5\Sigma^+$	1.873	490	3.11	0.93	1.881	484	3.07	0.92	523.5	19.9	8
$HeMn^{2+}$	$^6\Sigma^+$	1.996	383	2.45	0.92	2.004	380	2.43	0.92	415.2	17.7	7
$HeFe^{2+}$	$^5\Delta$	1.914	440	2.80	0.93	1.923	436	2.77	0.92	472.8	18.3	8
$HeCo^{2+}$	$^4\Phi$	1.838	490	3.07	0.94	1.840	484	3.11	0.92	525.9	25.5	6
$HeNi^{2+}$	$^3\Delta$	1.761	523	3.31	0.94	1.775	516	3.26	0.93	555.3	19.8	9
	$^3\Phi$	1.927	405	2.64	0.93	1.940	400	2.63	0.92	434.8	17.2	5
$HeCu^{2+}$	$^2\Sigma^+$	1.708	576	3.12	0.93	1.722	564	3.06	0.93	601.0	18.7	9
	$^2\Delta$	1.862	438	2.75	0.95	1.877	430	2.71	0.93	463.9	16.9	8
	$^2\Pi$	1.867	449	2.48	0.93	1.880	441	2.44	0.92	477.7	18.3	8

[a] Ratio of anharmonic variational $\nu_{1\rightarrow0}$ frequency to harmonic vibrational frequency. [b] The number of bound vibrational states determined from D_e, ω_e, $\omega_e x_e$, and $\omega_e y_e$.

occupation of the $3d_\pi$ orbitals for the $^2\Delta$ and $^2\Pi$ states is not significant in determining the order of these states.

For all $HeTM^{2+}$ species, a Mulliken population analysis of metal charge indicates that all species remain primarily TM^{2+} + He, even at the equilibrium bond length (Table 2). A decrease in helium electron donation is observed for electronic states with an occupied $3d_\sigma$ orbital. It is noted that the RKS−B3LYP method, while accurately predicting the molecular geometry, over-exaggerates the helium electron donation by about 0.05 electrons in comparison with the U_RCCSD(T) results.

The BSSE corrected D_e's (dissociating to He and TM^{2+}) are presented in Table 2. Additionally, for Co, Ni, and Cu the BSSE corrected D_e's for dissociation into the charge separated products $He^+ + TM^+$ are included in brackets. These charge separated products were found to be significantly higher in energy than the $He + TM^{2+}$ products, giving a large increase in dissociation energy. Hence, for all first row $HeTM^{2+}$, dissociation would be expected to yield $He + TM^{2+}$.

Trends in ground-state equilibrium bond lengths and D_e's are illustrated in Figure 2. A systematic decrease in equilibrium bond lengths for the ground electronic state was observed across the first row $HeTM^{2+}$. This would be expected, with increasing nuclear charge from Sc−Cu. However, occupation of the $3d_\sigma$ orbital increases inter-nuclear repulsion (TM-ligand repulsion) to the extent of altering this trend. The first species with an occupied $3d_\sigma$ orbital is $HeMn^{2+}$, which exhibits a bond lengthening of 0.123 Å over $HeCr^{2+}$.

The trends associated with the D_e of $HeTM^{2+}$ (illustrated in Figure 2b) reflect the bond length trends. An inverse (linear) relationship between bond length and D_e is expected and is observed for all species. Hence, Figure 2b confirms the trends observed in Figure 2a, in that occupation of the $3d_\sigma$ orbital in $HeMn^{2+}$ weakens the metal−ligand bond, causing a lengthening of R_e and a decrease in D_e.

The direct relationship between Figure 1 and Figure 2b and the inverse relationship between Figure 1 and Figure 2a further illustrates the significance of the 3*d* occupied orbital orientation (and the stability of a high-spin d^5 configuration). For the $HeTM^{2+}$, (Figure 2) three primary factors influence the trend in bond lengths. First, the increase in nuclear charge from Sc−Cu (and contraction of the 3*d* orbitals) increases attraction and shortens the bond length for $3d^n$ occupied states. Second, occupation of the antibonding $3d_\sigma$ (and 4*s*) orbital increases repulsion, and third, there is a preference for high-spin *d* orbital configurations. This preference for high-spin *d* orbital configurations can be seen to explain the trends observed in Figure 1 and Figure 2. For the atomic ion electronic transitions (Figure 1), an increase in nuclear charge produces a monotonic increase in the energy required to promote an electron to the 4*s* or 4*p* orbitals for the atomic ions with the exception that the reduction in transition energy from Mn^{2+} to Fe^{2+} is a direct result of stabilization of the $3d^5 4s^1$ and $3d^5 4p^1$ configurations relative to $3d^6$ configurations. For molecular D_e's, the stability of high-spin $3d^5$ configurations ensures occupation of the antibonding $3d_\sigma$ orbital, hence increasing R_e and lowering D_e between $HeCr^{2+}$ and $HeMn^{2+}$.

Müller, Tsong, and co-workers[13−15] have reported the experimental observation of HeV^{2+} and $HeFe^{2+}$. The dissociation energies of these two species in the ground electronic state were determined to be 30.5 and 32.8 kJ mol^{-1}, respectively. On this basis, it would be expected that $HeCr^{2+}$, $HeCo^{2+}$, $HeNi^{2+}$ and $HeCu^{2+}$, possessing greater D_e's, should be ready candidates for experimental observation. The remaining $HeSc^{2+}$, $HeTi^{2+}$, and $HeMn^{2+}$ (with lower D_e) may also be detectable, with $HeSc^{2+}$ the least likely.

It has been found that the BSSE is appreciable using the standard counterpoise method.[39] Employing basis sets such as Wachters+f[32,33] and Dunning's correlation consistent sets[29] made little difference to the BSSE. Hence, whereas the BSSE is appreciable, the observed trends in the ground-state D_e's are still expected to be valid. As a means of investigating the origin of the BSSE, frozen-core results were compared to all-electron results. The frozen-core (1*s*2*s*2*p*3*s*3*p* core) U_RCCSD(T) method produced a minimal BSSE, typically less than 1 kJ mol^{-1}. Moreover, lower D_e's were observed with the frozen-core approximation. For BSSE corrected D_e's, the all-electron and frozen-core (1*s*2*s*2*p*3*s*3*p* core) U_RCCSD(T) results were found to be almost identical, indicating that the difference in D_e between frozen-core and all-electron results is almost entirely due to BSSE. Hence, the BSSE corrected all-electron D_e's presented in Table 2 are expected to be reliable.

Potential energy functions for low-lying states of $HeTM^{2+}$ were constructed with a power series fit to discrete points typically in the range of 0.8 to 6.0 Å. Simons-Parr-Finlan expansion variables[41] were employed in all the power series fits. Series up to eighth order were used to ensure a minimal error to the fit. Vibrational frequencies were determined variationally from the potential curves and are presented in Table 3. Comparison of the variational anharmonic ν_{1-0} frequencies and the harmonic vibrational frequencies shows good agreement. With respect to the calculated harmonic frequencies, the usual ratio of 0.93 is evident between experimental and the ab initio

results.[44] For $HeNi^{2+}$ and $HeCu^{2+}$, selected low-lying electronic states were also investigated. The results correlate with ground state results, with a similar ratio of anharmonic to harmonic vibrational frequencies. Anharmonic constants determined from a fit to vibrational levels indicate a significant degree on anharmonicity. With the experimentally observed $HeFe^{2+}$ and HeV^{2+} possessing 8 and 7 bound vibrational levels, respectively, it would be expected that states with a similar number of bound levels should be ready targets for detection. On this premise, observation of $HeTi^{2+}$, $HeCr^{2+}$, $HeMn^{2+}$, $HeNi^{2+}$, and $HeCu^{2+}$ may be expected. $HeSc^{2+}$ and $HeCo^{2+}$ may also possibly be observed, with $HeSc^{2+}$ the least likely. These results support the analysis based on dissociation energies.

To examine the effect of relativistic corrections, the same sets of discrete points for each low-lying state were evaluated with the Cowan-Griffin one-electron operator and treated using a perturbational approach[42,43] within MOLPRO. Potential energy curves were fitted to these discrete points in the same manner as the nonrelativistic potentials. The equilibrium bond lengths, zero-point-energies, and lowest vibrational transitions including relativistic effects are listed in Table 3. The effect of relativity on equilibrium geometries and harmonic frequencies, as determined in the Cowan−Griffin scheme, is in the order of 0.01 Å and 5 cm^{-1}, respectively. This effect is shown to increase marginally in significance across the row Sc−Cu. Differential 3*d* and 4*s* relativistic effects are not observed due to the $3d^n$ configuration being the ground-state occupation exclusively.

Acknowledgment. We acknowledge the support of the Australian Research Council. Generous allocations of CPU resources were provided by APAC, ANUSF, AC^3, AINSE, and The University of Newcastle. D. J. D. W. acknowledges an Australian University of Newcastle Postgraduate Research Award.

References and Notes

(1) Hotokka, M.; Kindstedt, T.; Pyykko, P.; Roos, B. O. *Mol. Phys.* **1984**, *52*, 23.
(2) Partridge, H.; Bauschlicher, C. W. *J. Phys. Chem.* **1994**, *98*, 2301.
(3) Frenking, G.; Koch, W.; Liebman, J. F. *From Atoms to Polymers, Isoelectronic Analogies*; Liebman, J. F., Greenberg, A., Eds.; VCH Publishers: New York, 1989.
(4) Frenking, G.; Koch, W.; Cremer, D.; Gauss, J.; Liebman, J. F. *J. Phys. Chem.* **1989**, *93*, 3397.
(5) Frenking, G.; Koch, W.; Reichel, F.; Cremer, D. *J. Am. Chem. Soc.* **1990**, *112*, 4240.
(6) Frenking, G.; Cremer, D. *Struct. Bonding* **1990**, *73*, 17.
(7) Hughes, J. M.; von Nagy-Felsobuki, E. I. *Eur. Phys. J. D.* **1999**, *6*, 185.
(8) Hughes, J. M.; von Nagy-Felsobuki, E. I. *J. Mol. Struct. (THEOCHEM)* **1999**, *459*, 67.
(9) Wong, M. W.; Radom, L. *J. Am. Chem. Soc.* **1988**, *110*, 2375.
(10) Jemmis, E. D.; Wong, M. W.; Burgi, H.-B.; Radom, L. *J. Mol. Struct. (THEOCHEM)* **1996**, *261*, 385.
(11) Kemper, P. R.; Hsu, M.-T.; Bowers, M. T. *J. Phys. Chem.* **1991**, *95*, 10 600.
(12) von Helden, G.; Kemper, P. R.; Hsu, M.-T.; Bowers, M. T. *J. Chem. Phys.* **1992**, *96*, 6561.
(13) Müller, E. W.; Tsong, T. T. *Prog. Surf. Sci.* **1973**, *4*, 1.
(14) Tsong, T. T.; Kinkus, T. J. *Physica Scripta* **1983**, *T4*, 201.
(15) Müller, E. W.; McLane, S. B.; Panitz, J. A. *Surf. Sci.* **1969**, *17*, 430.
(16) Lessen, D.; Brucat, P. J. *J. Chem. Phys.* **1989**, *90*, 6296.
(17) Bauschlicher, C. W.; Langhoff, S. R.; Partridge, H. *Organometallic Ion Chemistry*, Edited by Freiser, B. S.; Kluwer: Netherlands, 1996; Chapter 2.
(18) Bauschlicher, C. W.; Partridge, H.; Langhoff, S. R. *J. Phys. Chem.* **1989**, *91*, 4733.
(19) Partridge, H.; Bauschlicher, C. W.; Langhoff, S. R. *J. Chem. Phys.* **1992**, *96*, 5350.
(20) Bauschlicher, C. W.; Partridge, H.; Langhoff, S. R. *Chem. Phys. Lett.* **1990**, *165*, 272.
(21) Bauschlicher, C. W.; Langhoff, S. R. *Int. Rev. Phys. Chem.* **1990**, *9*, 149.
(22) Niu, J.; Rao, B. K.; Jena, O.; Manninen, M. *Phys. Rev. B* **1995**, *51*, 4475.
(23) Harrison, J. *Chem. Rev.* **2000**, *100*, 679.
(24) Frisch, M. J.; Trucks, G. W.; Schlegel, H. B.; Scuseria, G. E.; Robb, M. A.; Cheeseman, J. R.; Zakrzewski, V. G.; Montgomery, J. A., Jr.; Stratmann, R. E.; Burant, J. C.; Dapprich, S.; Millam, J. M.; Daniels, A. D.; Kudin, K. N.; Strain, M. C.; Farkas, O.; Tomasi, J.; Barone, V.; Cossi, M.; Cammi, R.; Mennucci, B.; Pomelli, C.; Adamo, C.; Clifford, S.; Ochterski, J.; Petersson, G. A.; Ayala, P. Y.; Cui, Q.; Morokuma, K.; Malick, D. K.; Rabuck, A. D.; Raghavachari, K.; Foresman, J. B.; Cioslowski, J.; Ortiz, J. V.; Stefanov, B. B.; Liu, G.; Liashenko, A.; Piskorz, P.; Komaromi, I.; Gomperts, R.; Martin, R. L.; Fox, D. J.; Keith, T.; Al-Laham, M. A.; Peng, C. Y.; Nanayakkara, A.; Gonzalez, C.; Challacombe, M.; Gill, P. M. W.; Johnson, B. G.; Chen, W.; Wong, M. W.; Andres, J. L.; Head-Gordon, M.; Replogle, E. S.; Pople, J. A. *Gaussian 98*, revision A.7; Gaussian, Inc.: Pittsburgh, PA, 1998.
(25) Knowles, P. J.; Hampel, C.; Werner, H.-J. *J. Chem. Phys.* **1993**, *99*, 5219; Knowles, P. J.; Hampel, C.; Werner, H.-J. *J. Chem. Phys.* **2000**, *112*, 3106;
(26) Watts, J. D.; Gauss, J.; Bartlett, R. J. *J. Chem. Phys.* **1993**, *98*, 8718.
(27) MOLPRO is a package of ab initio programs written by H.-J. Werner and P. J. Knowles, with contributions by Amos, R. D.; Bernhardsson, A.; Berning, A.; Celani, P.; Cooper, D. L.; Deegan, M. J. O.; Dobbyn, A. J.; Eckert, F.; Hampel, C.; Hetzer, G.; Korona, T.; Lindh, R.; Lloyd, A. W.; McNicholas, S. J.; Manby, F. R.; Meyer, W.; Mura, M. E.; Nicklass, A.; Palmieri, P.; Pitzer, R.; Rauhut, G.; Schutz, M.; Stoll, H.; Stone, A. J.;Tarroni, R.; Thorsteinsson, T.
(28) Lee, T. J.; Rice, J. E.; Scuseria, C. E.; Schaefer, H. F. *Theor. Chim. Acta* **1989**, *75*, 81; Lee, T. J.; Taylor, P. R. *Int. J. Quantum Chem. Symp.* **1989**, *23*, 23.
(29) Woon, D. E.; Dunning, T. H. *J. Chem. Phys.* **1993**, *98*, 1358.
(30) Bederson, T. M.; Bederson, B. *Adv. At. Mol. Phys.* **1977**, *13*, 1.
(31) Bishop, D. M.; Pipin, J. J. Chem. Phys. **1989**, *91*, 3549.
(32) Moore, C. E. Atomic Energy Levels as Derived from the Analysis of Optical Spectra, *Nat. Stand. Ref. Data Ser. Nat. Bur. Stand.*, NSRDS−NBS, 1971.
(33) Wachter, A. J. *J. Chem. Phys.* **1970**, *52*, 1033.
(34) Bauschlisher, C. W.; Langhoff, S. R.; Barnes, L. A. *J. Chem. Phys.* **1989**, 91, 2399.
(35) Rappe, A. K.; Smedley, T. A.; Goddard, W. A. *J. Phys. Chem.* **1981**, *85*, 2607.
(36) Hay, P. J. *J. Chem. Phys.* **1977**, *66*, 4376.
(37) Langhoff, S. R.; Bauschlicher, C. W. *J. Chem. Phys.* **1986**, *84*, 4485.
(38) Almlof, J.; Taylor, P. R. *J. Chem. Phys.* **1987**, *86*, 4070.
(39) Schütz, M.; Lindh, R.; Werner, H.-J. *Mol. Phys.* **1999**, *96*, 719.
(40) Boys, S. F.; Bernardi, F. *Mol. Phys.* **1970**, *19*, 553.
(41) Searles, D. J.; von Nagy-Felsobuki, E. I. Ab Initio Variational Calculations of Molecular Vibrational−Rotational Spectra, *Lecture Notes in Chemistry*, **61**, Springer-Verlag: Berlin, 1993.
(42) Cowan, R. D.; Griffin, D. C. *J. Opt. Soc. Am.* **1976**, *66*, 1010.
(43) Martin, R. L. *J. Phys. Chem.* **1983**, *87*, 750.
(44) Hout, R. F.; Levi, B. A.; Hehre, W. J. *J. Comput. Chem.* **1982**, *3*, 234.